RSC Advances

PAPER

View Article Online
View Journal | View Issue

Cite this: *RSC Adv.*, 2024, **14**, 11311

Controlled delivery of 5-fluorouracil from monodisperse chitosan microspheres prepared by emulsion crosslinking

Tong Wan,[a] Qianqian Zhang,[a] Guocheng Jin[b] and Shiai Xu *[ac]

Received 22nd February 2024
Accepted 1st April 2024

DOI: 10.1039/d4ra01377h

rsc.li/rsc-advances

This work aims to determine the optimal conditions for emulsion cross-linking of chitosan (CHS) with various molecular weights using glutaraldehyde as a cross-linking agent to produce 5-fluorouracil-loaded CHS microspheres (5-FU/CHS). Their drug loading and encapsulation efficiencies are found to be in the range of 3.87–12.35% and 20.13–70.45%, respectively. The dynamic light scattering results show that 5-FU/CHS microspheres are micron-sized with a uniform size distribution, and the scanning electron microscopy results show that they are spherical. The results of thermogravimetric analysis, X-ray diffraction, and Fourier transform infrared spectroscopy demonstrate that 5-FU is successfully incorporated into the microspheres. The *in vitro* release tests show that 5-FU/CHS have a prolonged, pH-responsive release pattern of 5-FU, and the cumulative release rate under acidic condition is much larger than that under neutral conditions. The drug release kinetic analysis further demonstrates that the release of 5-FU can be well described by the Fickian diffusion model.

1. Introduction

To address the challenges posed by limited selectivity, high toxicity, and poor stability of anticancer drugs, numerous stimuli-responsive drug carriers have been developed to facilitate controlled drug release.[1,2] Drug release may be regulated by changing the pH, temperature, and magnetic field. Notably, the pH range in most tumor tissues (6.0–7.0) is different from that in normal tissues (7.4).[3] Capitalizing on microenvironmental disparities, many stimuli-responsive drug carriers are developed to improve the therapeutic efficacy and targeting. One of the most prescribed drugs for the treatment of solid tumors, such as colon, liver, lung, skin, and breast tumors, is 5-fluorouracil (5-FU), a fluorinated pyrimidine analogue.[4] However, its clinical use is somewhat limited because of the bioavailability, short half-life as a result of the quick metabolism of dihydropyrimidine dehydrogenase, and high systemic toxicity.[5] One promising solution to these problems is to oncorporate the drug into biodegradable polymeric microspheres. These carriers offer controlled drug release, bolstered tissue and cell selectivity, and augmented stability and bioavailability of encapsulated drugs. Many synthetic polymers, such as amino acid copolymers, polylactic acid and its copolymers, and polyvinyl alcohol, are used as drug carriers. Examples of natural polymers include gelatin, sodium alginate, shellac, albumin, and chitosan (CHS).[6]

CHS has proven to be a viable drug carrier because it is non-toxic, biocompatible, biodegradable, and antibacterial and allows for a delayed release of drugs in the form of capsules, microspheres, membranes, and fibers.[7–10] Due to their uniform particle size distribution and distinct morphology, CHS microspheres hold substantial promise across diverse biomedical applications,[11,12] and notably they display a pH-responsive drug release pattern and thus they can efficiently regulate drug release under various pH conditions.[8] The use of drug carriers with a uniform spherical shape and an appropriate particle size may substantially increase the drug delivery efficacy.[13,14] Hence, it is imperative to precisely control the morphology and particle size of CHS microspheres for biomedical drug delivery, given their pronounced impacts on factors such as the initial burst release, drug release kinetics, and dosing.[13] At present, CHS microspheres are often prepared by precipitation,[15] solvent volatilization,[16] spray drying,[17–19] and emulsion cross-linking.[20–23] Emulsion cross-linking is of special interest because it is controllable, simple, and repeatable. It consists of amalgamation of an aqueous-phase polymer (*e.g.*, CHS) dissolved in an oil-phase solution and an emulsion stabilizing surfactant.[24,25] Subsequently, the amino group of the polymer forms a linkage with its aldehyde counterpart in the presence of a cross-linking agent such as glutaraldehyde (GTA). Additionally, the surfactant influences surface tension, fostering the generation of spherical structures.[25] Challenges remain to maintain the stability of the emulsion and control the droplet size and uniform crosslinking for the preparation of

[a]*School of Materials Science and Engineering, East China University of Science and Technology, Shanghai 200237, China. E-mail: saxu@ecust.edu.cn*
[b]*Shanghai Flowridge Material Technology Co., Ltd, Shanghai 201318, China*
[c]*School of Chemical Engineering, Qinghai University, Xining 810016, China*

monodisperse microspheres by emulsion crosslinking. The particle size of the emulsion can be controlled by regulating the droplet size of the cross-linking agent, stirring rate, concentration, and other factors.

This study aims to examine how the molecular weight and concentration of CHS and GTA impact the preparation of 5-FU-loaded CHS (5-FU/CHS) microspheres by emulsion cross-linking and their effectiveness as drug carriers. The drug loading (DL) and encapsulation efficiencies (EE) were evaluated through centrifugation. The form and size of the drug-loaded microspheres were examined using dynamic light scattering (DLS) and scanning electron microscopy (SEM). The stability and drug encapsulation were evaluated by Fourier transform infrared spectroscopy (FTIR), X-ray diffraction (XRD), and thermogravimetric analysis (TGA). The *in vitro* drug release (IVDR) pattern and kinetics were evaluated by ultraviolet-visible (UV-vis) spectrophotometry.

2. Experimental

2.1 Materials

5-FU ($C_4H_3FN_2O_2$, 5-fluoropyrimidine-2,4-dione, ≥99%, biotech grade) powder was provided by Shanghai Macklin Biochemical Technology Co., Ltd (Shanghai, China). CHS ($(C_6H_{11}NO_4)_n$, (1,4)-2-amino-2-deoxy-β-D-glucan) of different molecular weights (773 000, 432 000 and 98 000 g mol^{-1}) with 80–90% deacetylation was obtained from Shanghai Aladdin Bio-Chem Technology Co., Ltd (Shanghai, China). Acetic acid, sorbitan monooleate (Span 80), glutaraldehyde (GTA, 50% purity), and anhydrous disodium hydrogen phosphate were purchased from Adamas Chemical Reagent Co., Ltd (Shanghai, China). Liquid paraffin, isopropanol, and anhydrous ethanol were purchased from General Reagent Co., Ltd (Shanghai, China). Purified water prepared using a Direct-Pure RO purified water system (5 μS cm^{-1}, RD0R01000, RephiLe Bioscience Co., Ltd, Shanghai, China) was used throughout the experiments. All reagents of analytical grade were employed without requiring further purification.

2.2 Preparation of 5-FU/CHS microspheres

5-FU/CHS microspheres were prepared by emulsion cross-linking (Fig. 1) using CHS of three molecular weights and concentrations (1, 2 and 3 wt%), 3 wt% of acetic acid, and 0.15 wt% of sodium hydroxide. 5-FU was added and cooked for 5 minutes at 40 °C. Liquid paraffin was added as an oil phase into a flask equipped with a high-speed homogenizer and Span 80 was added to create the W/O emulsion. A precise electric stirrer was used to agitate the aqueous and oil phase dispersions for 3 hours at 700 rpm. After stable emulsions were obtained, the pH of the solution was modulated to 4–5 using sodium hydroxide solution. Then, 4, 5, and 6 wt% of GTA solution was added dropwise with 5 wt% of isopropanol and continuously stirred. As a result, a total of 27 formulations were evaluated (Table 1). After 12 hours of continuous stirring at room temperature, the dispersion was centrifuged at 4000 rpm for 0.5 h. The oil phase on the surface of the microspheres was removed using a solvent after the removal of the supernatant. It was washed 6 times and centrifuged. To ensure that the mineral oil was completely removed, they were first cleaned with isopropyl alcohol and then with ethanol for three times. The samples were vacuum-dried at 40 °C to obtain 5-FU/CHS microspheres.

Table 1 Formulation numbers and compositions of 5-FU/CHS

Formulation	CHS Mw	CHS (wt%)	GTA (wt%)	Morphology
L14	Low	1	4	Irregular
L24		2		Irregular
L34		3		Irregular
L15		1	5	Spherical
L25		2		Spherical
L35		3		Spherical
L16		1	6	Aggregated
L26		2		Aggregated
L36		3		Aggregated
M14	Medium	1	4	Irregular
M24		2		Irregular
M34		3		Irregular
M15		1	5	Spherical
M25		2		Spherical
M35		3		Spherical
M16		1	6	Aggregated
M26		2		Aggregated
M36		3		Aggregated
H14	High	1	4	Irregular
H24		2		Irregular
H34		3		Irregular
H15		1	5	Spherical
H25		2		Spherical
H35		3		Spherical
H16		1	6	Aggregated
H26		2		Aggregated
H36		3		Aggregated

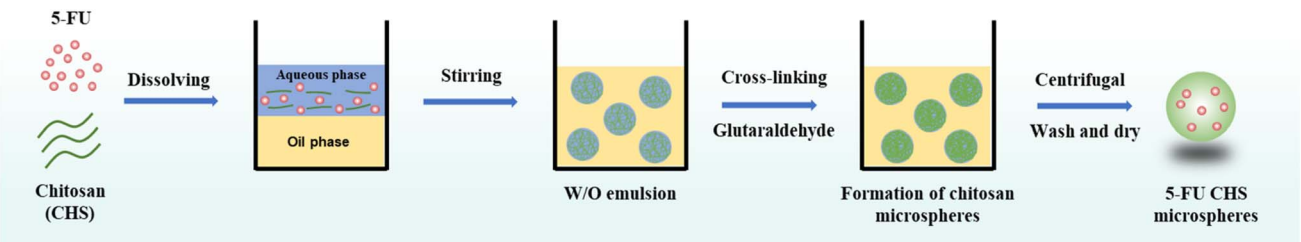

Fig. 1 Schematic illustration of the preparation of 5-FU/CHS microspheres.

2.3 Characterization of 5-FU/CHS

2.3.1 Evaluation of DL and EE. A solution comprising 1 mg of the sample was sonicated with 5 ml of 0.1 M HCl, followed by centrifugation. The resulting supernatant was diluted to 10 ml with 5 ml of freshly prepared 0.1 M HCl solution. An UV-2600i UV-vis spectrophotometer (Shimadzu, Japan) was employed to measure the absorbance of the clarified and diluted solution at 266 nm. The content of 5-FU was quantified by referencing the calibration curve derived from the absorbance of 5-FU at various concentrations. The adjusted values were calculated using CHS microspheres that were left empty. The measurement results were expressed as mean ± standard deviation (SD), with each measurement repeated in triplicate. DL and EE were calculated as follows:[13]

$$\mathrm{DL}(\%) = \frac{m_\mathrm{r}}{m_0} \times 100 \quad (1)$$

$$\mathrm{EE}(\%) = \frac{m_\mathrm{r}}{m_\mathrm{i}} \times 100 \quad (2)$$

where m_0 is the weight of the sample, m_r and m_i are the real and initial 5-FU weight of the sample, respectively.

2.3.2 SEM observation. The morphologies of pure CHS and 5-FU/CHS microspheres were observed by field emission electron scanning electron microscopy (FESEM, S-4800, Hitachi, Japan). The samples were dispersed in ethanol (1 mg ml^{-1}) to avoid agglomeration during drying. Then, the samples were fixed on a flat table with conductive adhesive, dried for 5 min, and placed in a sputter coater for gold spraying. The operating acceleration voltage was 15 kV and the beam current was 10 μA.

2.3.3 DLS analysis. The particle size distribution of 5-FU/CHS microspheres was determined using a laser particle size analyzer (S3500SI, Microtrac Inc., USA). Anhydrous ethanol was chosen as the ultrasonic dispersant.

2.3.4 FTIR spectroscopy. GTA, 5-FU, pure CHS, and selected 5-FU/CHS microspheres were characterized using FTIR spectroscopy (Nicolet 6700, Thermo Electron Corporation, USA) in a wavenumber range of 4000–400 cm^{-1}. The samples were pulverized into fine powder, blended with KBr, and then compacted to form discs.

2.3.5 XRD analysis. The physical properties of GTA, 5-FU, pure CHS, and selected 5-FU/CHS microspheres were evaluated utilizing XRD. The diffractograms were recorded with an X-ray diffractometer (Ultima IV, RIKEN, Japan) operating at 40 kV and 40 mA with Cu Kα as the radiation source, $\lambda = 1.54$ Å. The diffractograms angle (2θ) range was 5–65°, and the scanning speed was 4° min^{-1}.

2.3.6 TGA analysis. TGA curves were obtained by Perseus TG 209 F1 series thermal analysis system (NETZSCH, Germany). 5 mg of samples were meticulously measured and placed in a crucible affixed to a microbalance, and heated in the standard mode at a rate of 10 °C min^{-1} from 30 to 800 °C in a dry nitrogen atmosphere.

2.3.7 IVDR analysis. The IVDR was determined by dialysis. A beaker containing 50 ml of PB (pH 7.4 and pH 6.0) was filled with 5 mg of 5-FU/CHS previously wrapped in a dialysis bag (Viskase, USA; MD44-3.5, molecular weight cut-off 3500) and kept at 37 ± 0.5 °C at 100 rpm. Then, 5 ml of the solution to be analyzed was regularly taken from the conical flask. The release of 5-FU was quantified using UV-visible spectroscopy at 266 nm, and fresh PB was added in an equal volumetric ratio. Each measurement was repeated in triplicate, and the results were presented as mean ± SD. The proportion of instantaneous release for a given incubation period to the initial loading was defined as the cumulative release (CR), which was used to represent drug release:[13]

$$\mathrm{CR}(\%) = \frac{A_\mathrm{r}}{A_0} \times 100 \quad (3)$$

where A_0 represents the initial loading of 5-FU in CHS microspheres and A_r represents the quantity of 5-FU released at time t.

Table 2 Kinetic models used in this study

Model	Equation
Zero-order	$Q_t = Q_0 + K_0 t$
First-order	$\ln Q_t = \ln Q_0 + K_1 t$
Higuchi	$Q_t = C + K_\mathrm{H} t^{1/2}$
Hixson–Crowell	${Q_0}^{1/3} - {Q_t}^{1/3} = K_\mathrm{HC} t$
Korsmeyer–Peppas	$\frac{Q_t}{Q_\infty} = K_\mathrm{KP} t^n$

2.3.8 Drug release kinetics. The release mechanism of 5-FU from CHS microspheres was determined using five mathematical models of drug release kinetics (Table 2). Here, Q_t represents the cumulative release of 5-FU at time t, Q_0 represents the initial 5-FU release, and Q_t/Q_∞ indicates the percentage release of 5-FU. The constants K_0, K_1, K_H, K_HC, and K_KP represent the zero-order, first-order, Higuchi, Hixson–Crowell, and Korsmeyer–Peppas constants, respectively. The parameter n represents to the diffusion index. For the Korsmeyer–Peppas model, the release process is driven by Fickian diffusion ($n \leq 0.43$), non-Fickian diffusion ($0.43 < n < 0.85$), and matrix erosion ($n \geq 0.85$), respectively.[26]

3. Results and discussion

3.1 Preparation of 5-FU/CHS microspheres

CHS droplets were prepared by W/O emulsification. CHS was solubilized in a weakly acidic solution under shear stress in a continual oil phase and stirred by a continual stirrer to create droplets and to avoid fusion. The aqueous phase and the oil phase (5 wt% Span80-liquid paraffin solution) were respectively used to prepare W/O CHS droplets. To cross-link CHS, a GTA-5 wt% isopropanol solution was gently added using a peristaltic pump. The CHS solution and GTA were cross-linked to obtain CHS microspheres, as shown in Fig. 2. Schiff base reaction occurred when CHS solution droplets were brought into contact with GTA cross-linker droplets. The aldehyde and amino groups of the GTA molecules formed a dense structure as they diffused to the surface and interior of CHS droplets, and finally solid CHS microspheres were generated. Isopropanol was added to the cross-linker solution as a solvent to reduce the thickness of liquid paraffin, lower the surface tension of droplets, increase

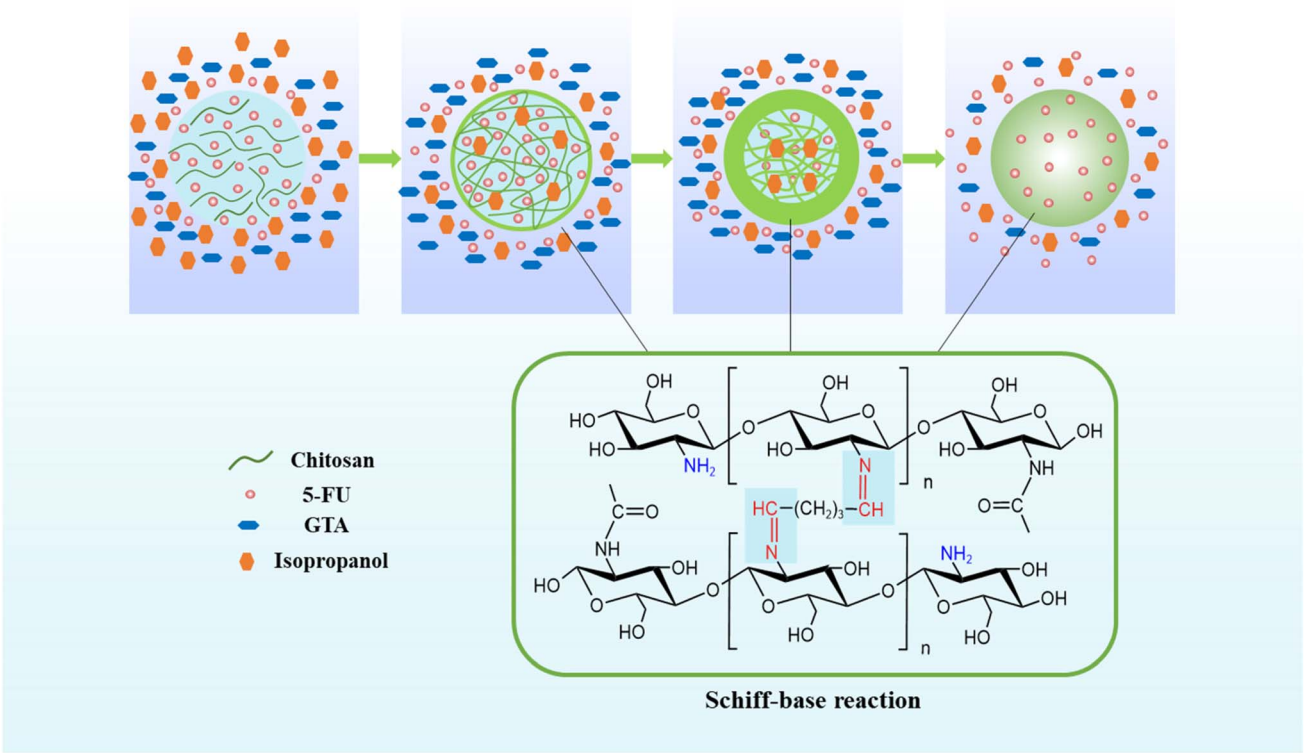

Fig. 2 Schematic illustration of the reaction of CHS and GTA to generate CHS microspheres.

Table 3 DL, EE, MS, and CV values of 5-FU/CHS microspheres

Formulation	DL% ± SD	EE% ± SD	MS (μm) ± SD	CV%
L15	3.87 ± 0.22	20.13 ± 1.10	0.75 ± 0.13	17.33
L25	4.32 ± 0.28	22.58 ± 1.40	1.13 ± 0.15	13.27
L35	7.84 ± 0.32	42.53 ± 1.61	1.69 ± 0.09	5.33
M15	3.96 ± 0.28	20.32 ± 1.40	18.84 ± 2.72	14.43
M25	5.98 ± 0.34	31.80 ± 1.71	21.60 ± 2.14	9.91
M35	9.63 ± 0.37	53.28 ± 1.86	26.90 ± 1.27	4.72
H15	4.38 ± 0.26	22.90 ± 1.30	46.15 ± 2.28	4.94
H25	6.19 ± 0.33	32.99 ± 1.66	61.48 ± 2.86	4.65
H35	12.35 ± 0.40	70.45 ± 2.01	79.17 ± 3.01	3.80

the diffusion of the cross-linking into the droplet and its interaction with CHS, and ultimately increase the cross-linker rate and homogeneity of CHS microspheres.[13] The solidified microspheres were centrifuged, filtered, cleaned, and vacuum-dried for 24 hours.

The prepared 5-FU/CHS microspheres are spherical, aggregated, or irregular in morphology, as shown in Table 1. Evidently, the development of CHS microspheres is influenced by GTA concentration. In order to precisely control the sizes of spherical microspheres, it is imperative to maintain the CHS and GTA concentrations within an optimal range. The findings indicate that CHS microspheres coalesce at a GTA concentration of 6 wt% but are irregular at a GTA concentration of 4 wt%. A low GTA concentration prevents the cross-linking of the aldehyde group with the amino group of CHS, forming asymmetric and weakly mechanically stable microspheres.[13] In this case, the loaded, 5-FU is very likely to slide off. However, the microspheres would adhere to one another more tightly at higher GTA concentrations, resulting in the formation of CHS microsphere aggregates. Thus, 5 wt% of GTA is the most appropriate concentration for cross-linking of CHS microspheres. Nine formulations with 5 wt% of GTA and 1, 2, and 3 wt% of CHS (low, medium, and high molecular weight) were chosen for future research based on the previous findings.

Table 4 DL and EE of 5-FU in various drug carriers

Drug carriers	Method	DL%	EE%	Reference
CHS microspheres	Emulsion cross-linking	12.35	70.45	This work
CHS nanoparticles	Emulsion cross-linking	1.43	58.90	8
CHS nanoparticles	Ionic gelation	7.26	42.15	9
CHS microspheres	Microfluidics	4.17	83.40	13
CHS/cerium oxide nanoparticles	Ionic gelation	9.65	95.18	28
Galactosylated CHS/bovine serum albumin microspheres	Emulsion cross-linking	2.90	40.30	29

3.2 Evaluation of DL and EE

The DL and EE of samples were determined by centrifugation. The data presented in Table 3 indicates that the DL of 5-FU/CHS microspheres ranges from 3.87% to 12.35% and the EE ranges from 20.13% to 70.45%, which are satisfactory compared to previous findings (Table 4). As shown in Fig. 3, both DL and EE increase with increasing molecular weight of CHS. For each molecular weight of CHS, both DL and EE increase with CHS concentration in the range of 1 wt% to 3 wt%. Notably, no substantial disparity in encapsulation efficiency (EE) is observed between low and high molecular weights of CHS, even when the CHS concentration increases from 1 wt% to 2 wt%. There is no significant difference in EE between low and high molecular weights of CHS as the CHS concentration increases from 1 wt% to 2 wt%. However, as the CHS concentration is further increased from 2 wt% to 3 wt%, the EE of all CHS increases significantly ($P < 0.05$). It is concluded that the molecular weight of CHS has a more pronounced effect on EE compared to its concentration. This finding is consistent with previous studies.[20] The increase in EE is attributed to the adsorption and electrostatic interactions between 5-FU and CHS.[27] The 5-FU/CHS microspheres prepared using 3 wt% of CHS and 5 wt% of GTA (L35, M35, and H35) show the highest drug loading capacity. It is also noted that all the three formulations are micron-sized with a low coefficient of variation

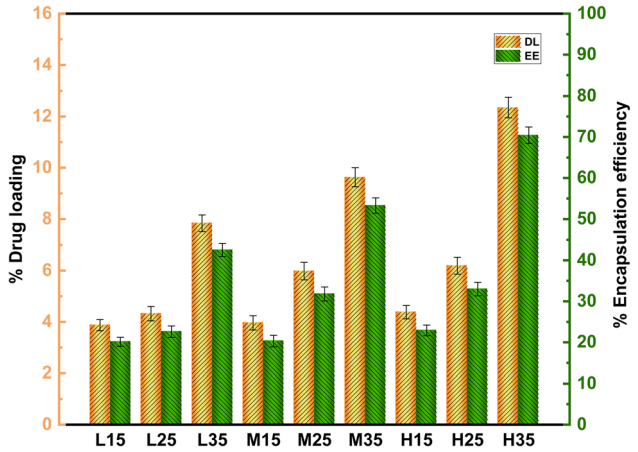

Fig. 3 Effect of molecular weight and concentration of CHS on DL and EE of 5-FU/CHS microspheres.

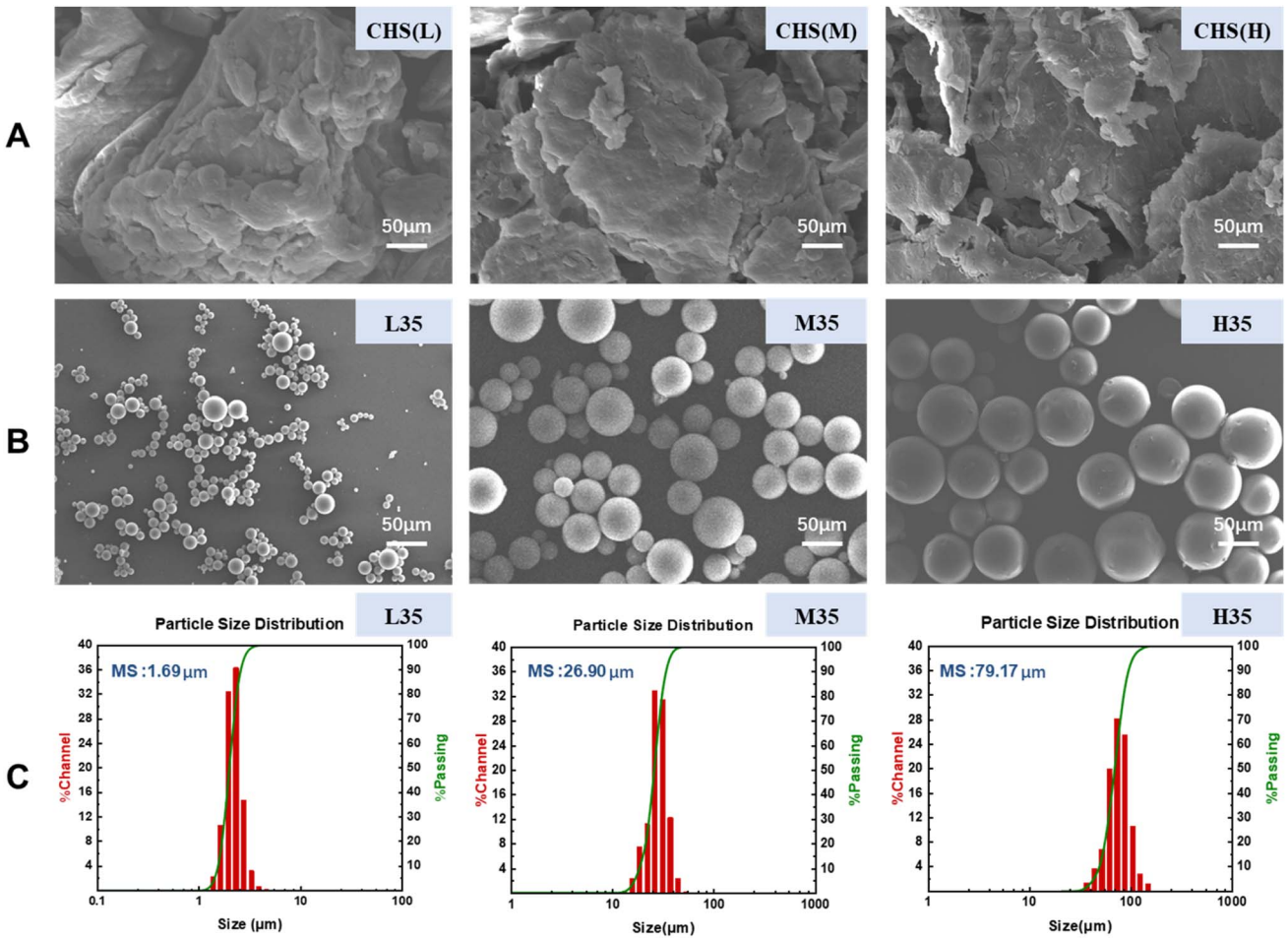

Fig. 4 Characterization of 5-FU/CHS microspheres: (A) SEM images of uncross-linked CHS, (B) SEM images of 5-FU/CHS microspheres, (C) size distribution of 5-FU/CHS microspheres.

(CV) (<5%), indicating that they are monodispersed in nature. Therefore, L35, M35, and H35 were selected for further studies.

3.3 SEM and DLS analysis

The morphology of CHS before and after cross-linking was observed by SEM, and the mean size (MS) and particle size distribution of 5-FU/CHS microspheres were analyzed by DLS. Table 3 shows the MS and CV values of nine 5-FU/CHS microspheres. It is found that the MS value ranges from 0.75 to 79.17 μm and it increases with increasing CHS concentration and molecular weight, which is likely linked to the viscosity of the CHS solution. The viscosity of the CHS solution is high when CHS has a high concentration or a high molecular weight, which can inhibit the generation of minute droplets during agitation and consequently results in formation of coarser emulsions and larger microspheres.[30,31] Fig. 4(A) shows that uncross-linked CHS(L) (low molecular weight CHS), CHS(M) (medium molecular weight CHS), and CHS(H) (high molecular weight CHS) have a blocky or flaky structure with poor regularity. Fig. 4(B) and (C) show that L35, M35, and H35 microspheres have smooth surface, good sphericity, and narrow particle size distribution, and they are monodispersed in nature with a MS value of 1.69 μm, 26.90 μm and 79.17 μm, respectively. The interpenetration of CHS and GTA culminates in the formation of a Schiff base through the interaction of the aldehyde group and amino group, consequently giving rise to the covalent cross-linking between GTA and CHS. As a consequence, the GTA cross-linked CHS microspheres have smooth surface, uniform particle dimensions, and favorable sphericity. In the development of nanoparticles, the smooth surface and chemical crosslinking of nanoparticles can enhance the maximum drug encapsulation.[8] The present study demonstrates that CHS microspheres are suitable for pharmacokinetic studies and have the potential to improve the bioavailability of 5-FU through the reduction of its toxicity.

3.4 FTIR spectroscopy

The FTIR spectra of the samples are shown in Fig. 5. Due to the stretching vibration of the O–H and N–H groups that are connected to the molecules through hydrogen bonds, the FTIR spectra of GTA exhibit large peaks in the range of 3000–3400 cm^{-1}.[32] The aldehyde group is responsible for the peak at 714 cm^{-1}, while the amide I (C=O) band and amide II (–NH) band are responsible for the two peaks at 1690 cm^{-1} and

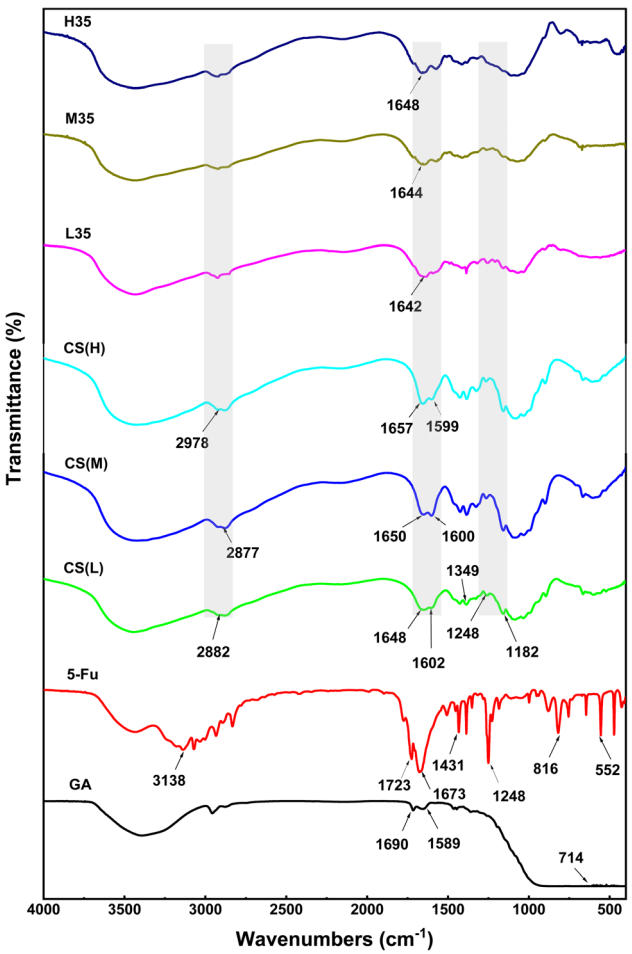

Fig. 5 FTIR spectra of GTA, 5-FU, CHS(L), CHS(M), CHS(H), and 5-FU/CHS microspheres (L35, M35, and H35).

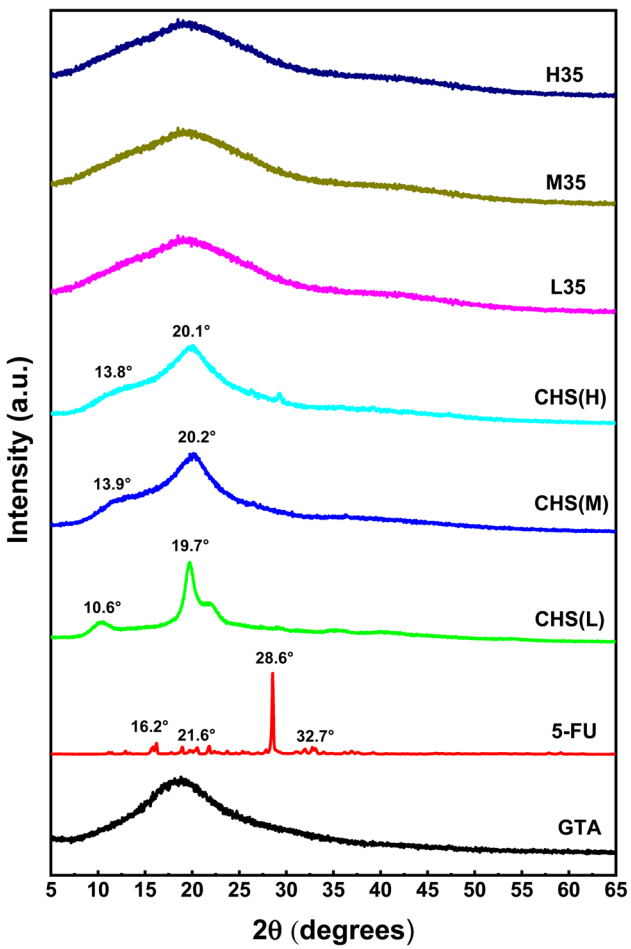

Fig. 6 XRD diffractograms of GTA, 5-FU, CHS(L), CHS(M), CHS(H), and 5-FU/CHS microspheres (L35, M35, and H35).

1589 cm^{-1}, respectively. Because of the vibration of the acyl (amide II and III) and aromatic ring, 5-FU displays strong peaks at 3138, 1723, 1673, 1431, 1248, 816, and 552 cm^{-1}, respectively. The spectral peaks in the range of 3071–2933 cm^{-1} are attributed to the stretching motion of –C–H bonds, whereas the peak at 1349 cm^{-1} corresponds to the vibrational activity of the pyrimidine moiety. The vibrations related to –C–O and –C–N are detected at 1182, 1673, and 1248 cm^{-1}. The chemical structures of CHS(L), CHS(M), and CHS(H) reveal distinct strong peaks associated with the N–H bending of amide I, at 1648, 1602, 1650, 1600 cm^{-1}, respectively. Similarly, the peaks related to the N–H bending of amide II are detected at 1657 and 1599 cm^{-1}. In pure CHS, distinct absorption bands related to C–N stretching are observed at 2882, 2877, and 2978 cm^{-1}, respectively.[33] Due to the strong covalent contacts between CHS and GTA, the peaks corresponding to the N–H stretching vibration in CHS are detected from 1657–1648 cm^{-1} to 1648–1642 cm^{-1} after covalent cross-linking and drug insertion, and the peak at 1602–1599 cm^{-1} is redshift. Evidently, the notable characteristic signal of 5-FU diminishes in the FTIR spectra of L35, M35, and H35, indicating intricate interaction between 5-FU and CHS molecules. Thus, 5-FU is effectively encapsulated in the produced microspheres.

3.5 XRD analysis

The XRD diffractograms of the samples are shown in Fig. 6. Only hump maps are seen in GTA with, no powerful distinctive peaks.[34–36] The strong diffraction peaks of CHS(L), CHS(M), and CHS(H) are observed at 10.6° and 19.7°, 13.9° and 20.2°, and 13.8° and 20.1°, respectively, demonstrating that CHS has a crystalline structure.[37] The crystalline-to-amorphous transition of CHS is indicated by the two large peaks at 19.7° and 42.1° in drug-loaded CHS microspheres (L35, M35, and H35) prepared using GTA as a cross-linking agent. Because CHS molecular chains are less flexible and less regularly spaced after cross-linking, the crystallinity of drug-loaded CHS microspheres is lower than that of pure CHS.[29] Because the stiffness of CHS microspheres is stabilized by intramolecular and intermolecular covalent connections between the aldehyde group of GTA

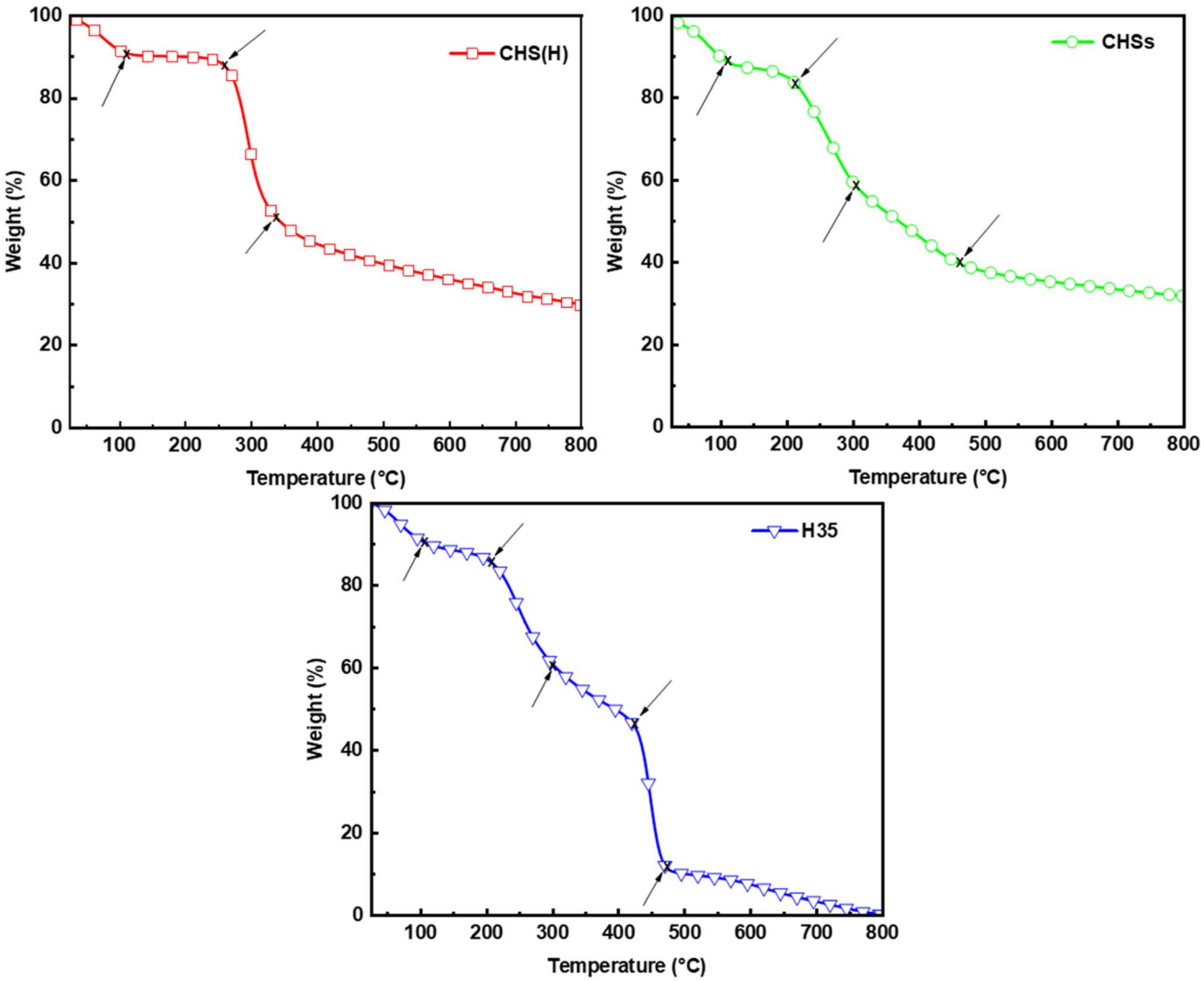

Fig. 7 TGA curves of CHS(H), CHSs and H35.

and the amino group of CHS,[35] the change in 2θ proves the efficient cross-linking of GTA.[38] A single sharp peak is seen at 2θ of 28.6°in 5-FU, indicating that it is crystalline. The presence of several moderately intense diffraction peaks at 2θ of 16.2°, 19.8°, 21.6°, 22.4°, 32.7°, 36.5°, 36.8°, and 46.6° reveals the crystalline nature of the drug. Although both the polymer and the drug show sharp peaks, the distinctive peak associated with 5-FU is absent in drug-loaded CHS microspheres, indicating that the carrier has been successfully incorporated in an amorphous form.[39,40] This results in the hysteresis of the pores and the interaction between the polymer network and the cross-linker. Similar findings are also obtained in previous studies.[8,41]

3.6 TGA analysis

The TGA results of CHS(H), drug-unloaded CHS microspheres (CHSs) and H35 are shown in Fig. 7. CHS(H), CHSs, and H35 exhibit three, four, and five weight-loss stages in the temperature range of 30–800 °C in nitrogen, respectively. At around 100 °C, a weight loss of about 10% can be seen for all samples, which is attributed to moisture loss. CHS experiences the second weight-loss stage (37%) at 252 °C due to the breakage of the ether bond within CHS(H), and the third weight-loss stage (20%) at 336 °C due to the decomposition of glucose units.[42,43] For CHSs, the second weight-loss stage starts earlier than CHS(H) at around 205 °C with a weight loss of about 30%, which is attributed to the breakage of the ether bond of CHS. The third weight-loss stage occurs at 314 °C with an 18% reduction in weight, which is attributed to the breakage of the covalent bonds formed between CHS and GTA. At the fourth weight-loss stage, the decomposition of glucose units in CHSs starts at 476 °C, which is later than that of CHS(H) due to the enhanced molecular interactions between polymer chains after cross-linking of CHSs by GTA. This observation aligns with the findings from SEM, FTIR, and XRD analyses. The second, third, and fifth weight-loss stages of H35 are basically consistent with that of CHSs, and the fourth weight-loss stage occurs at 424 °C with a 35% reduction in weight, which is due to the phase transition temperature of 5-FU and thus indicates that CHS microspheres are successfully loaded with 5-FU. These results suggest that drug-loaded CHS microspheres exhibit good stability under normal physiological conditions.

3.7 IVDR analysis

The acidic condition of tumor tissues and the neutral condition of normal tissues were simulated under pH 6.0 and 7.4, respectively, and the drug release characteristics of free 5-FU and 5-FU/CHS microspheres (L35, H35, and M35) in PB are shown in Fig. 8. It is found that free 5-FU exhibits rapid release into pH 6.0 and 7.4 buffers within 5 hours, as shown by the steep curves in Fig. 8, while 5-FU/CHS microspheres exhibit a sustained release pattern consistent with controlled release systems.[44,45] As a result of the dissolution of unencapsulated 5-FU from microspheres within the first hour, a modest amount of 5-FU is released suddenly from samples. According to Fig. 8 and Table 5, the maximal cumulative releases (CRs) of 5-FU in L35, M35, and H35 after 96 hours of incubation are 82.52%, 74.46%, and 70.54% at pH = 6.0, and are 55.68%, 48.65%, and 44.54% at pH = 7.4, respectively. Compared to the neutral condition, the release rate and CRs of 5-FU are elevated under

Table 5 Maximum cumulative drug release of three 5-FU/CHS microspheres under different pH conditions

		CRs (%)	
Formulation	MS (μm) ± SD	pH 6.0	pH 7.4
L35	1.69 ± 0.09	82.52 ± 0.82	55.68 ± 0.86
M35	26.90 ± 1.27	74.46 ± 0.69	48.65 ± 0.84
H35	79.17 ± 3.01	70.54 ± 0.80	44.54 ± 0.96

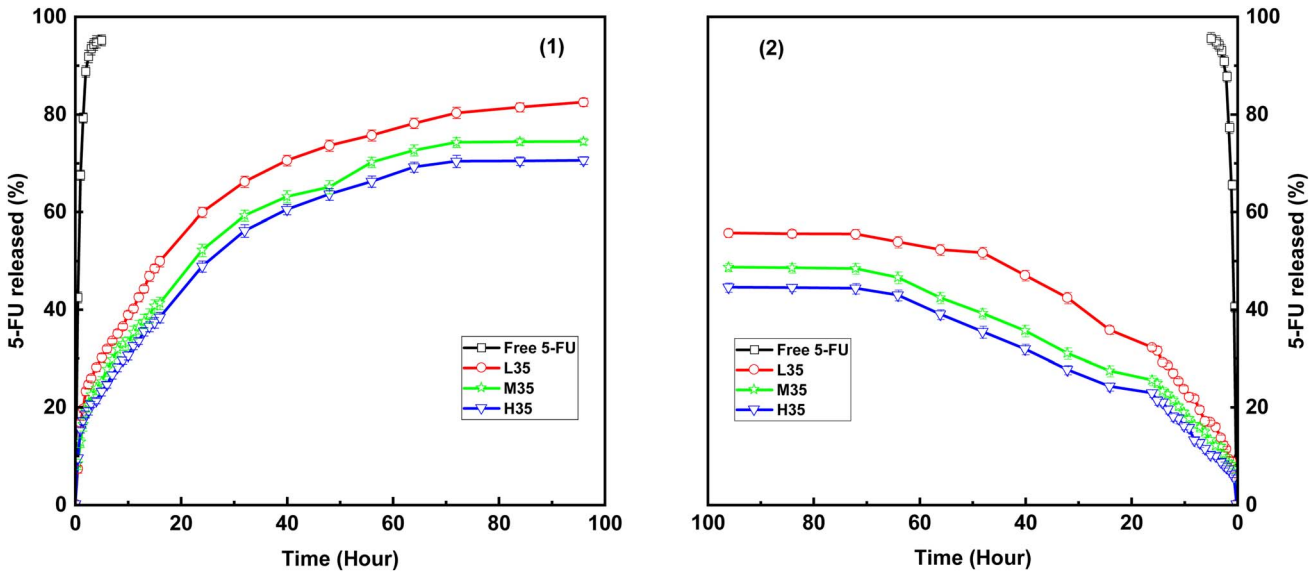

Fig. 8 IVDR from free 5-FU and three 5-FU/CHS microspheres in different pH conditions: (1) pH 6.0, (2) pH 7.4.

Table 6 Parameters and correlation coefficients of *in vitro* release kinetic models

		Zero-order		First-order		Higuchi		Hixson–Crowell		Korsmeyer–Peppas	
Formulation	pH	K_0	R^2	K_1	R^2	K_H	R^2	K_{HC}	R^2	n	R^2
L35	6.0	0.7724	0.7993	0.0755	0.9343	8.5334	0.9560	0.004	0.8653	0.3309	0.9244
	7.4	0.5683	0.8323	0.0592	0.9686	6.1998	0.9692	0.0025	0.8732	0.3787	0.9417
M35	6.0	0.7264	0.8287	0.0056	0.9385	7.9402	0.9691	0.0035	0.8856	0.3583	0.9367
	7.4	0.4873	0.8944	0.0512	0.9370	5.1842	0.9883	0.0020	0.9194	0.4192	0.9604
H35	6.0	0.6941	0.8414	0.0626	0.9314	7.5366	0.9705	0.0033	0.8939	0.3769	0.9423
	7.4	0.4636	0.9027	0.0442	0.9565	4.9075	0.9873	0.0019	0.9258	0.4285	0.9574

the acidic condition. This effect can be ascribed to increased permeability of CHS microsphere walls due to amine protonation and CHS degradation. For CHS-based delivery devices, similar drug release behaviors have also been reported in the literature.[46–49] These findings imply that 5-FU/CHS microspheres have a pH-responsive drug release pattern.

Table 5 also shows that the CRs values of 5-FU/CHS microspheres decrease with increasing CHS molecular weight. According to earlier DLS findings, the particle size of CHS microspheres grows with CHS molecular weight, which can affect the length of the drug diffusion channel.[13,50] Consequently, drug release can be controlled by altering the particle sizes of the microspheres. Fig. 8 shows that the monodisperse CHS microspheres have good controlled drug–release properties due to the extremely slow and sustained release pattern of 5-FU. Thus, monodisperse CHS microspheres have a greater potential to extend the pharmacological action of 5-FU and to increase the therapeutic efficacy than previously described nano/microspheres.[29,51]

3.8 Drug release kinetics

Five kinetic models, including zero-level, first-level, Higuchi, Hixson–Crowell, and Korsmeyer–Peppas models, were examined to understand the release process of 5-FU from CHS microspheres.[52–55] Table 6 demonstrates that the Higuchi model has the largest correlation coefficient, indicating that 5-FU/CHS microspheres exhibit diffusion-based kinetics.[56] The results are analyzed using the Korsmeyer–Peppas equation, and the release index "n" is calculated to further investigate the drug release mechanism. According to the Korsmeyer–Peppas theory, $n \leq 0.43$ indicates that the release follows Fickian mechanism, $0.43 < n < 0.85$ indicates that the release follows anomalous (non-Fickian) diffusion, $n = 0.85$ indicates migration in the second case (zero-level release), while $n > 0.85$ indicates migration in the super-second case.[57] As shown in Table 6, the n values are less than 0.43, indicating Fickian diffusion.

4. Conclusion

The purpose of this study are to prepared 5-FU/CHS microspheres by emulsion cross-linking and to investigate how the molecular weight, concentration, and GTA and CHS quantities influence the preparation and properties of these microspheres. At 5 wt% of GTA, the prepared CHS microspheres are spherical with a uniform particle size distribution. The monodisperse 5-FU/CHS microspheres display good DL, prolonged pH-responsive drug release, and high EE. Higher CHS concentrations can enhance the drug encapsulation efficiency, while higher CHS molecular weights can enhance the microsphere size. A CHS concentration of 3 wt% results in the best drug loading performance. The FTIR, XRD and TGA results demonstrate the effective incorporation of 5-FU into the carrier. The TGA findings indicate that 5-FU/CHS microspheres are very stable. The diffusion kinetic model shows the biphasic (abrupt and slow) drug release of 5-FU. The release of the drug may be slowed down by using CHS with a high molecular weight. These findings help us prepare CHS-based polymeric microspheres for more effective transport of 5-FU. To sum up, 5-FU/CHS microspheres are expected to have significant potential for the delivery of drug in the field of anticancer therapeutics.

Author contributions

Tong Wan: investigation, methodology, data curation, validation, formal analysis, visualization, writing – original draft. Qianqian Zhang: methodology, data curation, visualization. Guocheng Jin: project administration, resources, funding acquisition. Shiai Xu: conceptualization, project administration, resources, writing – review & editing, supervision, funding acquisition.

Conflicts of interest

There are no conflicts to declare.

Acknowledgements

This research is financially supported by the Shanghai Flowridge Material Technology Co., LTD

References

1 L. Shang, X. Jiang, T. Yang, H. Xu, Q. Xie, M. Hu, C. Yang, L. Kong and Z. Zhang, *Acta Pharm. Sin. B*, 2022, **12**, 2550–2567.
2 X. Sun, C. Liu, A. M. Omer, L.-Y. Yang and X.-k. Ouyang, *Int. J. Biol. Macromol.*, 2019, **132**, 487–494.

3 X. C. Zheng, W. Ren, S. Zhang, T. Zhong, X. C. Duan, Y. F. Yin, M. Q. Xu, Y. L. Hao, Z. T. Li, H. Li, M. Liu, Z. Y. Li and X. Zhang, *Int. J. Nanomed.*, 2018, **13**, 1495–1504.
4 M. Samy, S. H. Abd El-Alim, A. E. G. Rabia, A. Amin and M. M. H. Ayoub, *Int. J. Biol. Macromol.*, 2020, **156**, 783–791.
5 S. Khan, A. Madni, H. Shah, N. Jan, A. Shafiq, A. Basit, N. Rai, A. Ali and M. M. Khan, *Int. J. Biol. Macromol.*, 2022, **222**, 497–508.
6 T. K. Mwangi, I. M. Berke, E. H. Nieves, R. D. Bell, S. B. Adams and L. A. Setton, *J. Controlled Release*, 2018, **283**, 76–83.
7 A. M. dos Santos, S. G. Carvalho, L. M. B. Ferreira, M. Chorilli and M. P. D. Gremião, *Colloids Surf., A*, 2022, **640**, 128417.
8 A. Sethi, M. Ahmad, T. Huma and W. Ahmad, *Drug Delivery*, 2021, **28**, 1569–1584.
9 L. Sun, Y. Chen, Y. Zhou, D. Guo, Y. Fan, F. Guo, Y. Zheng and W. Chen, *Asian J. Pharm. Sci.*, 2017, **12**, 418–423.
10 S. Zhong, H. Zhang, Y. Liu, G. Wang, C. Shi, Z. Li, Y. Feng and X. Cui, *Carbohydr. Polym.*, 2017, **168**, 282–289.
11 W. Wei, G.-H. Ma, L.-Y. Wang, J. Wu and Z.-G. Su, *Acta Biomater.*, 2010, **6**, 205–209.
12 J. Wu, W. Wei, L.-Y. Wang, Z.-G. Su and G.-H. Ma, *Colloids Surf., B*, 2008, **63**, 164–175.
13 T. He, W. Wang, B. Chen, J. Wang, Q. Liang and B. Chen, *Carbohydr. Polym.*, 2020, **236**, 116094.
14 D. Y. Pratt, L. D. Wilson and J. A. Kozinski, *J. Colloid Interface Sci.*, 2013, **395**, 205–211.
15 Y.-W. Liu, Y. Zhou, G.-Q. Huang, L.-P. Guo, X.-D. Li and J.-X. Xiao, *Food Chem.*, 2022, **385**, 132689.
16 S. Shi, S. Song, X. Liu, G. Zhao, F. Ding, W. Zhao, S. Zhang, Y. Song and W. Ma, *Drug Delivery*, 2022, **29**, 548–560.
17 H. Bhatt, J. Bahadur, R. Checker, P. Ajgaonkar, S. R. Vishwakarma and D. Sen, *Colloids Surf., B*, 2021, **208**, 112067.
18 D. R. Fonseca, A. Moura, V. Leiro, R. Silva-Carvalho, B. N. Estevinho, C. L. Seabra, P. C. Henriques, M. Lucena, C. Teixeira, P. Gomes, P. Parreira and M. C. L. Martins, *Acta Biomater.*, 2022, **137**, 186–198.
19 Q. Zhang, Y. Du, M. Yu, L. Ren, Y. Guo, Q. Li, M. Yin, X. Li and F. Chen, *Carbohydr. Polym.*, 2022, **277**, 118880.
20 M. He, H. Wang, W. Dou, G. Chou, X. Wei and Z. Wang, *Int. J. Biol. Macromol.*, 2016, **91**, 1101–1109.
21 G. Wang, J. Wang, Z. Chen and J. Hu, *Int. J. Biol. Macromol.*, 2022, **206**, 232–241.
22 X. Zhang, Y. Pan, S. Li, L. Xing, S. Du, G. Yuan, J. Li, T. Zhou, D. Xiong, H. Tan, Z. Ling, Y. Chen, X. Hu and X. Niu, *Int. J. Biol. Macromol.*, 2020, **164**, 2204–2214.
23 X. Zhou, M. Kong, X. Cheng, J. Li, J. Li and X. Chen, *Colloids Surf., B*, 2014, **123**, 387–394.
24 Y. Beldengrün, J. Aragon, S. F. Prazeres, G. Montalvo, J. Miras and J. Esquena, *Langmuir*, 2018, **34**, 9731–9743.
25 A. A. Cerón, L. Nascife, S. Norte, S. A. Costa, J. H. Oliveira do Nascimento, F. D. P. Morisso, J. Baruque-Ramos, R. C. Oliveira and S. M. Costa, *Int. J. Biol. Macromol.*, 2021, **185**, 572–581.
26 N. A. Peppas and J. J. Sahlin, *Int. J. Pharm.*, 1989, **57**, 169–172.
27 A. Mehrotra, R. C. Nagarwal and J. K. Pandit, *Chem. Pharm. Bull.*, 2011, **59**, 315–320.
28 A. Sathiyaseelan, K. Saravanakumar and M.-H. Wang, *Int. J. Biol. Macromol.*, 2022, **216**, 52–64.
29 C. Zhang, Y. Cheng, G. Qu, X. Wu, Y. Ding, Z. Cheng, L. Yu and Q. Ping, *Carbohydr. Polym.*, 2008, **72**, 390–397.
30 G. C. Bazzo, E. Lemos-Senna and A. T. N. Pires, *Carbohydr. Polym.*, 2009, **77**, 839–844.
31 C. J. Thompson, D. Hansford, S. Higgins, C. Rostron, G. A. Hutcheon and D. L. Munday, *Int. J. Pharm.*, 2007, **329**, 53–61.
32 M. Li, S. K. Cushing, J. Zhang, J. Lankford, Z. P. Aguilar, D. Ma and N. Wu, *Nanotechnology*, 2012, **23**, 115501.
33 Q. Gan, T. Wang, C. Cochrane and P. McCarron, *Colloids Surf., B*, 2005, **44**, 65–73.
34 E. Fournier, C. Passirani, N. Colin, P. Breton, S. Sagodira and J.-P. Benoit, *Eur. J. Pharm. Biopharm.*, 2004, **57**, 189–197.
35 A. Jain, K. Thakur, P. Kush and U. K. Jain, *Int. J. Biol. Macromol.*, 2014, **69**, 546–553.
36 P. Mukhopadhyay, S. Chakraborty, S. Bhattacharya, R. Mishra and P. P. Kundu, *Int. J. Biol. Macromol.*, 2015, **72**, 640–648.
37 Y. Zhang, Y. Yang, K. Tang, X. Hu and G. Zou, *J. Appl. Polym. Sci.*, 2008, **107**, 891–897.
38 Y. Yuan, B. M. Chesnutt, G. Utturkar, W. O. Haggard, Y. Yang, J. L. Ong and J. D. Bumgardner, *Carbohydr. Polym.*, 2007, **68**, 561–567.
39 A. E. Ashour, M. Badran, A. Kumar, T. Hussain, I. A. Alsarra and A. E. B. Yassin, *Int. J. Nanomed.*, 2019, **14**, 9259–9273.
40 M. Nasr, M. K. Ghorab and A. Abdelazem, *Acta Pharm. Sin. B*, 2015, **5**, 79–88.
41 S. Papadimitriou, D. Bikiaris, K. Avgoustakis, E. Karavas and M. Georgarakis, *Carbohydr. Polym.*, 2008, **73**, 44–54.
42 S. Tripathi, G. K. Mehrotra and P. K. Dutta, *Int. J. Biol. Macromol.*, 2009, **45**, 372–376.
43 X.-F. Zhao, Z.-J. Li, L. Wang and X.-J. Lai, *J. Appl. Polym. Sci.*, 2008, **109**, 2571–2575.
44 R. S. Bhatta, H. Chandasana, Y. S. Chhonker, C. Rathi, D. Kumar, K. Mitra and P. K. Shukla, *Int. J. Pharm.*, 2012, **432**, 105–112.
45 Y. Yu, R. Feng, S. Yu, J. Li, Y. Wang, Y. Song, X. Yang, W. Pan and S. Li, *Int. J. Biol. Macromol.*, 2018, **114**, 462–469.
46 T. Li, J. Yang, R. Liu, Y. Yi, M. Huang, Y. Wu, H. Tu and L. Zhang, *Int. J. Biol. Macromol.*, 2019, **126**, 68–73.
47 S. Song, Y. Wang, J. Xie, B. Sun, N. Zhou, H. Shen and J. Shen, *ACS Appl. Mater. Interfaces*, 2019, **11**, 34258–34267.
48 N. K. Verma, M. P. Purohit, D. Equbal, N. Dhiman, A. Singh, A. K. Kar, J. Shankar, S. Tehlan and S. Patnaik, *Bioconjugate Chem.*, 2016, **27**, 2605–2619.
49 Q. Xu, M. Hashimoto, T. T. Dang, T. Hoare, D. S. Kohane, G. M. Whitesides, R. Langer and D. G. Anderson, *Small*, 2009, **5**, 1575–1581.
50 C. Stewart, A. Siu, C. Tsui, Y. Finer and B. Hatton, *J. Mater. Chem. B*, 2022, **10**, 6453–6463.
51 A. M. Puga, A. C. Lima, J. F. Mano, A. Concheiro and C. Alvarez-Lorenzo, *Carbohydr. Polym.*, 2013, **98**, 331–340.

52 J. Dredán, R. Zelkó, I. Antal, E. Bihari and I. Rácz, *Int. J. Pharm.*, 1998, **160**, 257–260.
53 A. Sood and R. Panchagnula, *Int. J. Pharm.*, 1998, **175**, 95–107.
54 M. L. Vueba, L. A. E. Batista de Carvalho, F. Veiga, J. J. Sousa and M. E. Pina, *Eur. J. Pharm. Biopharm.*, 2004, **58**, 51–59.
55 A. Yeop, J. Sandanasamy, S. F. Pang and J. Gimbun, *Food Biosci.*, 2021, **41**, 101025.
56 R. S. Tığlı Aydın and M. Pulat, *J. Nanomater.*, 2012, **2012**, 313961.
57 K. Kheiri, N. Sohrabi, R. Mohammadi and M. S. Amini-Fazl, *Int. J. Biol. Macromol.*, 2022, **202**, 191–198.